

Research paper

# Complex patterns in a space- and time-discrete predator-prey model with Beddington-DeAngelis functional response



Tousheng Huang, Huayong Zhang\*, Hongju Yang, Ning Wang, Feifan Zhang

Research Center for Engineering Ecology and Nonlinear Science, North China Electric Power University, Beijing 102206, P.R. China

---

## ARTICLE INFO

**Article history:**

Received 30 November 2015

Revised 27 May 2016

Accepted 4 July 2016

Available online 6 July 2016

---

**Keywords:**

Pattern formation

Turing instability

Hopf bifurcation

Spatiotemporal chaos

---

## ABSTRACT

The spatial pattern formation of predator-prey systems is an important issue widely concerned. In this research, we address this issue by developing a new space- and time-discrete predator-prey model, with predation relationship described by Beddington-DeAngelis functional response. The discrete model is given by a coupled map lattice, taking a nonlinear relationship between predator-prey “reaction” stage and dispersal stage. Through analysis of Turing instability and Hopf instability for the discrete model, the parametric conditions for pattern formation are determined. Numerical simulations reveal a surprising variety of spatiotemporal patterns, including regular and irregular patterns of spots, stripes, labyrinth, gaps, mosaics, spirals, circles, and many intermediate patterns in-between. These patterns cover a majority of predator-prey pattern types recorded in literature. Besides, the discrete model predicts the occurrence of spatiotemporal chaos, which is responsible for the formation of irregular patterns. This research demonstrates that the nonlinear mechanisms of the discrete model better capture the complexity of pattern formation of predator-prey systems.

© 2016 Elsevier B.V. All rights reserved.

---

## 1. Introduction

Spatial pattern formation is one of the important and timely central topics in biological science [1–3]. It explains the self-organized spatial heterogeneity of populations and communities and plays a key role in understanding the dynamical complexity of biological systems. As recorded in literature, the spatial patterns widely exist in reality and manifest in a variety of complex types, such as vegetation stripes in semiarid regions, spots in vertebrate skins, and spiral waves in population distributions [3–6]. In recent decades, the complexity of spatial patterns has aroused more and more interests of theoretical and experimental biologists [7–9].

Predator-prey system is a type of basic biological system in nature. Due to its universal existence and importance, the dynamical behaviors of predator-prey system are investigated by a great number of researchers [10–14]. For a predator-prey system characterized by nonlinear interactions and spatial heterogeneity, spatiotemporal complexity of the system often exhibits [8,15,16]. Various approaches to modeling have been developed to enable the understanding of spatial pattern formations ranging from plant distributions to plankton aggregation [11,16,40–42]. According to the results of former research works [15–19], complex spatial predator-prey patterns are found, such as patterns of spots, stripes, labyrinth, and so on. The complexity of pattern formation in the predator-prey systems may arise in part from the diversity of predation relationships,

---

\* Corresponding author. Fax: 86-010-80799258.

E-mail address: [rceens@ncepu.edu.cn](mailto:rceens@ncepu.edu.cn) (H. Zhang).

and also from the complexity of nonlinear mechanisms. Predictably, the spatiotemporal complexity of predator-prey systems will continue to be one of the dominant themes in biology.

In the previous studies, most of the spatially extended models recorded in literature researching the predator-prey pattern formations are time- and space-continuous. However the continuous dynamic models hardly describe the discontinuity in the predator-prey systems, which may result from, for example, patchy environment or fragmented habitat [8,20]. For discontinuous predator-prey systems, applying discrete models should be more reasonable and adequate [8]. It is widely recognized that discrete dynamic models have advantage in describing nonlinear characteristics and complexity of natural ecological systems, compared with the continuous models. Domokos and Scheuring [21] found that the discrete model can be more accurate than corresponding continuous model in describing population dynamics. Complex nonlinear characteristics can emerge in the discrete model, including flip bifurcation, quasiperiodic behavior, chaos, and so on [22–24]. A lot of research works have demonstrated that the application of discrete dynamic models can lead to better results in studying predator-prey systems [25]. As found by Neubert et al., in comparing with the continuous reaction-diffusion models in which the conditions for diffusive instability are surprisingly severe, the discrete models exhibit dispersal-driven instability under a broader set of ecological conditions [37]. Such result can also be supported by the research of Han et al. [33].

The most common discrete models in literature developed for spatially extended systems are cellular automata and coupled map lattices [8,26,38,39,43,44]. In this research, the space- and time-discrete predator-prey model will be given by a coupled map lattice. The coupled map lattices are characterized by discrete time, discrete space, and continuous states. Compared with cellular automata, the coupled map lattices have great advantages in describing the spatiotemporal chaos and are widely applied in many fields [27]. In biology, the application of coupled map lattices results in a better understanding and prediction of biological complexity of pattern formations [8,9,27]. However, few coupled map lattice models are documented in literature for quantitatively describing the pattern formation of predator-prey systems. Applying the coupled map lattice models favours the understanding on the formation of complex patterns in predator-prey systems.

In this research, a space- and time-discrete predator-prey model, which is given by a coupled map lattice, is developed to study the pattern formation of a predator-prey system. The research is organized as follows. Section 2 gives the development of the discrete model, in which the predation relationship is described by Beddington-DeAngelis functional response. Section 3 provides the pattern formation conditions, via analyzing Hopf instability and Turing instability of the discrete model. In Section 4, numerical simulations are performed to show the complex patterns. Section 5 discusses the ecological significances of the results obtained, and finally, conclusions are made in Section 6.

## 2. Development of space- and time-discrete predator-prey model

The development of the space- and time-discrete predator-prey model is based on two aspects, (1) discretization of a continuous predator-prey model which is described by reaction-diffusion equations, and (2) application of the framework of a coupled map lattice. Accordingly, the former continuous predator-prey model should be introduced at first.

Generally, a classical spatially extended predator-prey model, which is mostly widely applied in literature, can be described by the following reaction-diffusion equations [15,16,28]:

$$\frac{\partial N}{\partial t} = Nf(N) - Pg(N, P) + d_1 \nabla^2 N, \quad (1a)$$

$$\frac{\partial P}{\partial t} = \varepsilon Pg(N, P) - \eta P + d_2 \nabla^2 P, \quad (1b)$$

in which  $N$  and  $P$  are both spatiotemporal variables, meaning prey and predator densities, respectively;  $t$  denotes time;  $f(N)$  describes the prey growth rate;  $g(N, P)$  is the functional response describing the predation relationship, e.g., the prey consumption rate by an average single predator;  $\varepsilon$  is the conversion rate of eaten prey into new predator abundance;  $\eta$  is the per capita predator death rate;  $\nabla^2 N$  and  $\nabla^2 P$  express the diffusion of the prey and the predator in space,  $d_1$  and  $d_2$  are diffusion coefficients; specially,  $\nabla^2 = \partial/\partial x^2 + \partial/\partial y^2$  is the usual Laplacian operator in two-dimensional space,  $x$  and  $y$  give the space coordinates of  $N$  and  $P$ .

Many functions for  $f$  and  $g$  can be found in literature [29]. In this research, we focus on the following  $f$  and  $g$ :

$$f(N) = r \left(1 - \frac{N}{K}\right), \quad (2a)$$

$$g(N, P) = \frac{\beta N}{B + N + wP}, \quad (2b)$$

which have been studied by many researchers [15–19]. In Eqs. (2),  $r$  stands for maximum per capita growth rate of the prey;  $K$  is the carrying capacity;  $\beta$  is the maximum consumption rate;  $B$  is a half-saturation constant;  $w$  is the predator interference parameter. With such  $f$  and  $g$ , Eqs. (1) describe a spatially extended predator-prey model with Beddington-DeAngelis functional response. According to the investigation in literature, this model exhibits a few spatial patterns, such as spotted pattern, labyrinth pattern, pattern of labyrinth with spots, and so on [15].

The new discrete model is developed based on discretizing the above continuous predator-prey model. For discretizing the continuous model, we consider a time interval  $\tau$  and a space interval  $h$ , and a two-dimensional rectangular domain

which includes  $n \times n$  grid elements (notice that the length of each grid element is  $h$ ). Each grid element represents one site and is ascribed to two numbers, i.e., the prey density and the predator density. The prey and predator densities in each site can change with time in the course of the system dynamics, due to the local inter- and intra-specific interactions as well as migration or dispersal between different sites. On this basis, we define two state variables in the discrete space and time,  $N_{(i,j,m)}$  and  $P_{(i,j,m)}$  ( $i, j \in \{1, 2, 3, \dots, n\}$  and  $m \in \mathbb{Z}^+$ ), which represent the prey density and the predator density in  $(i, j)$  site and at  $m$ th iteration (with initial time  $t_0$ , the time at  $m$ th iteration is  $t_0 + m\tau$ ).

With such discrete variables defined and applying the discretization of the continuous model, the discrete model can now be developed. In this research, the discrete model is given by a coupled map lattice. For the framework of coupled map lattice, one can refer to Mistro et al. [8], Punithan et al. [9], Rodrigues et al. [27], Kaneko [38], and Solé et al. [39]. In the coupled map lattice, the dynamics at each discrete step from  $m$  to  $m+1$  consists of two distinctly different stages, (a) the dispersal stage and (b) the “reaction” stage [8]. The dispersal stage can be obtained by discretizing the spatial terms of Eqs. (1), i.e.,

$$N'_{(i,j,m)} = N_{(i,j,m)} + \frac{\tau}{h^2} d_1 \nabla_d^2 N_{(i,j,m)}, \quad (3a)$$

$$P'_{(i,j,m)} = P_{(i,j,m)} + \frac{\tau}{h^2} d_2 \nabla_d^2 P_{(i,j,m)}, \quad (3b)$$

where  $\nabla_d^2$  here denotes the discrete form of the Laplacian operator, and

$$\nabla_d^2 N_{(i,j,m)} = N_{(i+1,j,m)} + N_{(i-1,j,m)} + N_{(i,j+1,m)} + N_{(i,j-1,m)} - 4N_{(i,j,m)}, \quad (4a)$$

$$\nabla_d^2 P_{(i,j,m)} = P_{(i+1,j,m)} + P_{(i-1,j,m)} + P_{(i,j+1,m)} + P_{(i,j-1,m)} - 4P_{(i,j,m)}, \quad (4b)$$

where dispersal is limited to the nearest neighbors. According to Mistro et al. [8], the reaction stage is described by

$$N_{(i,j,m+1)} = f_1(N'_{(i,j,m)}, P'_{(i,j,m)}), \quad (5a)$$

$$P_{(i,j,m+1)} = g_1(N'_{(i,j,m)}, P'_{(i,j,m)}). \quad (5b)$$

where  $f_1$  and  $g_1$  are functions determined by the local inter- and intra-specific interactions. In this research, these two functions can be obtained via discretizing the non-spatial part of Eqs. (1) [22,23], i.e.,

$$f_1(N, P) = N + \tau \left( rN \left( 1 - \frac{N}{K} \right) - \frac{\beta NP}{B + N + wP} \right), \quad (6a)$$

$$g_1(N, P) = P + \tau \left( \frac{\varepsilon \beta NP}{B + N + wP} - \eta P \right). \quad (6b)$$

The combination of Eqs. (3~6) describes the space- and time- discrete predator-prey model with Beddington–DeAngelis functional response [15,17,19]. For ecological significance, all the parameters used in the discrete model are positive and the values of  $N_{(i,j,m)}$  and  $P_{(i,j,m)}$  are nonnegative. Notice that the above discrete model cannot describe the dynamics on the boundary. For applying the discrete model, boundary conditions must be provided. In this research, we set periodic boundary conditions as the following,

$$N_{(i,0,m)} = N_{(i,n,m)}, \quad N_{(i,1,m)} = N_{(i,n+1,m)}, \quad N_{(0,j,m)} = N_{(n,j,m)}, \quad N_{(1,j,m)} = N_{(n+1,j,m)}, \quad (7a)$$

$$P_{(i,0,m)} = P_{(i,n,m)}, \quad P_{(i,1,m)} = P_{(i,n+1,m)}, \quad P_{(0,j,m)} = P_{(n,j,m)}, \quad P_{(1,j,m)} = P_{(n+1,j,m)}. \quad (7b)$$

In the following, the discrete model is employed to investigate the spatial pattern formation of predator and prey. For this purpose, the conditions for pattern formation should be determined.

### 3. Conditions for pattern formation

We focus on the pattern formation resulting from symmetry breaking at the stable spatially homogeneous state. There are two types of symmetry breaking, temporal symmetry breaking and spatial symmetry breaking. Temporal symmetry breaking is induced by Hopf bifurcation, giving rise to states that are homogeneous in space and oscillatory in time; whereas spatial symmetry breaking is induced by Turing bifurcation, leading to the formation of patterns that are stationary in time and oscillatory in space [15]. When temporal and spatial symmetry breakings take place simultaneously, the discrete model will generate the patterns that are oscillatory in both space and time.

Therefore, the determination of pattern formation conditions includes three parts.

- (1) Conditions for stable homogeneous stationary state: a nontrivial homogeneous stationary state exists and is stable to spatially homogeneous perturbations.
- (2) Conditions for Hopf instability: the stable stationary state becomes unstable due to Hopf bifurcation.
- (3) Conditions for Turing instability: the stable stationary state is unstable to at least one type of spatially heterogeneous perturbation, due to Turing bifurcation.

### 3.1. Conditions for stable homogeneous stationary state

The conditions for stable homogeneous stationary state are obtained firstly. The homogeneous stationary states of the discrete model suggest

$$\nabla_d^2 N_{(i,j,m)} = 0, \quad (8a)$$

$$\nabla_d^2 P_{(i,j,m)} = 0, \quad (8b)$$

for all of  $i$  and  $j$ . In such case, the equations of the discrete model changes into the following:

$$N_{(i,j,m+1)} = N_{(i,j,m)} + \tau \left( rN_{(i,j,m)} \left( 1 - \frac{N_{(i,j,m)}}{K} \right) - \frac{\beta N_{(i,j,m)} P_{(i,j,m)}}{B + N_{(i,j,m)} + wP_{(i,j,m)}} \right), \quad (9a)$$

$$P_{(i,j,m+1)} = P_{(i,j,m)} + \tau \left( \frac{\varepsilon \beta N_{(i,j,m)} P_{(i,j,m)}}{B + N_{(i,j,m)} + wP_{(i,j,m)}} - \eta P_{(i,j,m)} \right). \quad (9b)$$

Mathematically, the stationary states of the discrete model are represented by the fixed points of Eqs. (9). According to the definition of fixed point [30], the fixed points of Eqs. (9) are solved by

$$N = N + \tau \left( rN \left( 1 - \frac{N}{K} \right) - \frac{\beta NP}{B + N + wP} \right), \quad (10a)$$

$$P = P + \tau \left( \frac{\varepsilon \beta NP}{B + N + wP} - \eta P \right). \quad (10b)$$

Calculation on Eqs. (10) obtains three nonnegative fixed points,

$$(N_0, P_0) : (0, 0), \quad (11a)$$

$$(N_1, P_1) : (K, 0), \quad (11b)$$

$$(N_2, P_2) : \left( \frac{K}{2rw\varepsilon}, \frac{K(\beta\varepsilon - \eta)}{2rw^2\varepsilon\eta} C - \frac{B}{w} \right), \quad (11c)$$

in which

$$C = rw\varepsilon - \beta\varepsilon + \eta + \sqrt{(rw\varepsilon - \beta\varepsilon + \eta)^2 + \frac{4rwB\varepsilon\eta}{K}}. \quad (12)$$

Each of the above three fixed points represents a spatially homogeneous stationary state of the discrete model. In the following, the stability of the spatially homogeneous stationary states with respect to spatially homogeneous perturbations is analyzed. For spatially homogeneous perturbations, Eqs. (8) still establish. Hence, Eqs. (9) can still be applied to study the stability of the spatially homogeneous stationary states. Applying the Jacobian matrix of Eqs. (9),

$$J(N, P) = \begin{pmatrix} 1 + \tau \left( r \left( 1 - \frac{2N}{K} \right) - \frac{\beta P(B + wP)}{(B + N + wP)^2} \right) & - \frac{\beta \tau N(B + N)}{(B + N + wP)^2} \\ \frac{\beta \tau \varepsilon P(B + wP)}{(B + N + wP)^2} & 1 + \tau \left( \frac{\beta \varepsilon N(B + N)}{(B + N + wP)^2} - \eta \right) \end{pmatrix}. \quad (13)$$

Substituting the values of  $(N_0, P_0)$ ,  $(N_1, P_1)$ ,  $(N_2, P_2)$  as described in (11) into (13), then we have the Jacobian matrix for each fixed point. Calculating the two eigenvalues of the Jacobian Matrix,  $\lambda_1$  and  $\lambda_2$ . According to literature [30], the following criterion can be described: if  $|\lambda_1| < 1$  and  $|\lambda_2| < 1$ , then the corresponding fixed point is a stable node or a stable focus; if  $|\lambda_1| > 1$  and  $|\lambda_2| > 1$ , then the corresponding fixed point is an unstable node or an unstable focus; if  $|\lambda_1| > 1$  and  $|\lambda_2| < 1$  or  $|\lambda_1| < 1$  and  $|\lambda_2| > 1$ , then the corresponding fixed point is a saddle point, which is also unstable.

It is easy to find that the two eigenvalues of  $J(N_0, P_0)$  are  $1 + r\tau$  and  $1 - \tau\eta$ , and that one of the eigenvalues,  $1 + r\tau$ , is larger than one. Therefore  $(N_0, P_0)$  is unstable according to the above criterion. As well, calculating the two eigenvalues of  $J(N_1, P_1)$ , we find that when

$$0 < r\tau < 2 \text{ and } \frac{\beta\varepsilon K}{B + K} < \eta < \frac{2}{\tau} + \frac{\beta\varepsilon K}{B + K}, \quad (14)$$

the absolute values of the two eigenvalues are less than 1 and therefore  $(N_1, P_1)$  is stable. Following the same procedure, the conditions under which  $(N_2, P_2)$  is stable can be expressed as the following:

$$a_{11} + a_{22} < 1 + a_{11}a_{22} - a_{12}a_{21}, \quad (15a)$$

$$a_{11} + a_{22} > -(1 + a_{11}a_{22} - a_{12}a_{21}), \quad (15b)$$

$$a_{11}a_{22} - a_{12}a_{21} < 1, \quad (15c)$$

in which

$$a_{11} = 1 + r\tau \left(1 - \frac{2N_2}{K}\right) - \frac{a_{21}}{\varepsilon}, \quad (16a)$$

$$a_{12} = -\frac{\tau\eta^2}{\beta\varepsilon^2} \left(1 + \frac{B}{N_2}\right), \quad (16b)$$

$$a_{21} = \frac{r^2\tau\varepsilon}{\beta} \left(w + \frac{B}{P_2}\right) \left(1 - \frac{N_2}{K}\right)^2, \quad (16c)$$

$$a_{22} = 1 - \tau\eta + a_{12}\varepsilon. \quad (16d)$$

When  $(N_1, P_1)$  is stable, the predator-prey system will converge to the state where predator is extinct and prey exists only. The extinction of predator in this state suggests absence of the “reaction” stage, which leads to no pattern formation. Thereinafter, we merely focus on the pattern formation at stable  $(N_2, P_2)$ .

### 3.2. Conditions for Hopf instability

The conditions of existence of Hopf bifurcation are determined by the Hopf bifurcation theorem in [31]. Since the Hopf bifurcation is space-independent, Eqs. (9) can be used to study the Hopf bifurcation for the discrete model. The discrete model may undergo the Hopf bifurcation at  $(N_2, P_2)$  when any one of the parameters in Eqs. (9) varies. To show an example, the Hopf bifurcation corresponding to the variation of parameter  $\tau$  is studied in this subsection. The two eigenvalues  $\lambda_1$  and  $\lambda_2$  of the Jacobian matrix (13) associated with  $(N_2, P_2)$  are

$$\lambda_{1,2} = \frac{1}{2} \left( a_{11} + a_{22} \pm \sqrt{(a_{11} - a_{22})^2 + 4a_{12}a_{21}} \right), \quad (17)$$

The first condition for the occurrence of Hopf bifurcation is that  $\lambda_1$  and  $\lambda_2$  are a pair of conjugate complex numbers with modulus one. When  $(a_{11} - a_{22})^2 + 4a_{12}a_{21} < 0$ , i.e.,

$$\begin{aligned} & \left( r\tau \left(1 - \frac{2N_2}{K}\right) - \frac{r^2\tau}{\beta} \left(w + \frac{B}{P_2}\right) \left(1 - \frac{N_2}{K}\right)^2 + \tau\eta + \frac{\tau\eta^2}{\beta\varepsilon} \left(1 + \frac{B}{N_2}\right) \right)^2 \\ & - 4 \frac{r^2\tau^2\eta^2}{\beta^2\varepsilon} \left(1 + \frac{B}{N_2}\right) \left(w + \frac{B}{P_2}\right) \left(1 - \frac{N_2}{K}\right)^2 < 0, \end{aligned} \quad (18)$$

$\lambda_1$  and  $\lambda_2$  are complex. When  $a_{11}a_{22} - a_{12}a_{21} = 1$ , i.e.,

$$\tau = \tau_0 = \frac{r \left(1 - \frac{2N_2}{K}\right) - \frac{r^2}{\beta} \left(w + \frac{B}{P_2}\right) \left(1 - \frac{N_2}{K}\right)^2 - \eta - \frac{\eta^2}{\beta\varepsilon} \left(1 + \frac{B}{N_2}\right)}{\left(r \left(1 - \frac{2N_2}{K}\right) - \frac{r^2}{\beta} \left(w + \frac{B}{P_2}\right) \left(1 - \frac{N_2}{K}\right)^2\right) \left(\eta + \frac{\eta^2}{\beta\varepsilon} \left(1 + \frac{B}{N_2}\right)\right) - \frac{r^2\eta^2}{\beta^2\varepsilon} \left(1 + \frac{B}{N_2}\right) \left(w + \frac{B}{P_2}\right) \left(1 - \frac{N_2}{K}\right)^2}, \quad (19)$$

we have  $|\lambda_1| = |\lambda_2| = 1$ .

We translate the point  $(N_2, P_2)$  to the origin by the translation

$$u = N - N_2, \quad (20a)$$

$$v = P - P_2. \quad (20b)$$

With the translation, a map is obtained from Eqs. (9), described as

$$\begin{pmatrix} u \\ v \end{pmatrix} \rightarrow \begin{pmatrix} a_{11}u + a_{12}v + \frac{a_{13}}{2}u^2 + a_{14}uv + \frac{a_{15}}{2}v^2 + \frac{a_{16}}{6}u^3 + \frac{a_{17}}{2}u^2v + \frac{a_{18}}{2}uv^2 + \frac{a_{19}}{6}v^3 + O((|u| + |v|)^4) \\ a_{21}u + a_{22}v + \frac{a_{23}}{2}u^2 + a_{24}uv + \frac{a_{25}}{2}v^2 + \frac{a_{26}}{6}u^3 + \frac{a_{27}}{2}u^2v + \frac{a_{28}}{2}uv^2 + \frac{a_{29}}{6}v^3 + O((|u| + |v|)^4) \end{pmatrix} \quad (21)$$

in which  $a_{11}, a_{12}, a_{21}, a_{22}$  are described by Eqs. (16),  $O((|u| + |v|)^4)$  describes a function with order at least four in the

variables  $(u, v)$ , and

$$\begin{aligned} a_{13} &= -\frac{2r\tau}{K} + \frac{2\beta\tau P_2(B+wP_2)}{(B+N_2+wP_2)^3}, \quad a_{14} = -\frac{\beta\tau(B^2+BN_2+BwP_2+2wN_2P_2)}{(B+N_2+wP_2)^3}, \\ a_{15} &= \frac{2w\beta\tau N_2(B+N_2)}{(B+N_2+wP_2)^3}, \quad a_{16} = -\frac{6\beta\tau P_2(B+wP_2)}{(B+N_2+wP_2)^4}, \\ a_{17} &= \frac{2\beta\tau(B^2+BN_2+2wN_2P_2-w^2P_2^2)}{(B+N_2+wP_2)^4}, \\ a_{18} &= \frac{2\beta\tau w(B^2+BwP_2+2wN_2P_2-N_2^2)}{(B+N_2+wP_2)^4}, \quad a_{19} = -\frac{6w^2\beta\tau N_2(B+N_2)}{(B+N_2+wP_2)^4}, \\ a_{23} &= -\varepsilon\left(a_{13} + \frac{2r\tau}{K}\right), \quad a_{24} = -\varepsilon a_{14}, \quad a_{25} = -\varepsilon a_{15}, \quad a_{26} = -\varepsilon a_{16}, \quad a_{27} = -\varepsilon a_{17}, \quad a_{28} = -\varepsilon a_{18}, \quad a_{29} = -\varepsilon a_{19}. \end{aligned} \quad (22)$$

Under the conditions (18) and (19), the eigenvalues of the Jacobian matrix associated with map (21) at the fixed point  $(0, 0)$  are also conjugate complex numbers with modulus 1. The two eigenvalues are written as

$$\lambda(\tau_0), \bar{\lambda}(\tau_0) = \frac{-p(\tau_0)}{2} \pm \frac{i'}{2}\sqrt{4q(\tau_0) - p^2(\tau_0)} = \alpha_1 \pm i'\alpha_2, \quad (23)$$

in which  $i' = \sqrt{-1}$  and

$$p(\tau_0) = -2 - r\tau_0\left(1 - \frac{2N_2}{K}\right) + \eta\tau_0 + \frac{\beta\tau_0(BP_2 - \varepsilon BN_2 + wP_2^2 - \varepsilon N_2^2)}{(B+N_2+wP_2)^2}, \quad (24a)$$

$$\begin{aligned} q(\tau_0) &= 1 + \tau_0\left(r\left(1 - \frac{2N_2}{K}\right) - \frac{\beta P_2(B+wP_2)}{(B+N_2+wP_2)^2} + \frac{\beta\varepsilon N_2(B+N_2)}{(B+N_2+wP_2)^2} - \eta\right) \\ &\quad + \tau_0^2\left(r\left(1 - \frac{2N_2}{K}\right)\frac{\beta\varepsilon N_2(B+N_2)}{(B+N_2+wP_2)^2} + \frac{\beta\eta P_2(B+wP_2)}{(B+N_2+wP_2)^2} - r\eta\left(1 - \frac{2N_2}{K}\right)\right). \end{aligned} \quad (24b)$$

Then we have

$$|\lambda| = \sqrt{q(\tau_0)}, \quad (25)$$

and need

$$\begin{aligned} d &= \frac{d|\lambda(\tau)|}{d\tau} \Big|_{\tau=\tau_0} = -\frac{1}{2}\left(r\left(1 - \frac{2N_2}{K}\right) - \frac{\beta P_2(B+wP_2)}{(B+N_2+wP_2)^2} + \frac{\beta\varepsilon N_2(B+N_2)}{(B+N_2+wP_2)^2} - \eta\right) \\ &= \frac{rN_2}{2K^2\beta P_2}(K\beta P + r(w\varepsilon - 1)(K - N_2)^2) \neq 0. \end{aligned} \quad (26)$$

In addition, the occurrence of the Hopf bifurcation also requires

$$(\lambda(\tau_0))^{\theta} \neq 1, \theta = 1, 2, 3, 4, \quad (27)$$

which is equivalent to

$$p(\tau_0) \neq -2, 0, 1, 2. \quad (28)$$

It should be noticed that in Eq. (23),  $p^2(\tau_0) \neq 4$ . Hence,  $p(\tau_0) \neq -2, 2$ , then the requirement of  $p(\tau_0) \neq 0, 1$  leads to

$$\frac{\beta\tau_0(1-w\varepsilon)N_2P_2}{(B+N_2+wP_2)^2} - \frac{r\tau_0N_2}{K} \neq -3, -2. \quad (29)$$

Next the normal form of (21) when  $\tau = \tau_0$  is studied. Applying the transformation

$$\begin{pmatrix} u \\ v \end{pmatrix} = \begin{pmatrix} a_{12} & 0 \\ \alpha_1 - a_{11} & -\alpha_2 \end{pmatrix} \begin{pmatrix} U \\ V \end{pmatrix} \quad (30)$$

to map (21), then the map becomes

$$\begin{pmatrix} U \\ V \end{pmatrix} \rightarrow \begin{pmatrix} \alpha_1 & -\alpha_2 \\ \alpha_2 & \alpha_1 \end{pmatrix} \begin{pmatrix} U \\ V \end{pmatrix} + \frac{1}{a_{12}\alpha_2} \begin{pmatrix} F_1(U, V) \\ G_1(U, V) \end{pmatrix}, \quad (31)$$

where

$$\begin{aligned} F_1(U, V) = & \frac{a_{13}\alpha_2}{2}u^2 + a_{14}\alpha_2uv + \frac{a_{15}\alpha_2}{2}v^2 + \frac{a_{16}\alpha_2}{6}u^3 + \frac{a_{17}\alpha_2}{2}u^2v \\ & + \frac{a_{18}\alpha_2}{2}uv^2 + \frac{a_{19}\alpha_2}{6}v^3 + O((|U| + |V|)^4), \end{aligned} \quad (32a)$$

$$\begin{aligned} G_1(U, V) = & \left(\frac{a_{13}(\alpha_1 - a_{11})}{2} - \frac{a_{12}a_{23}}{2}\right)u^2 + (a_{14}(\alpha_1 - a_{11}) - a_{12}a_{24})uv \\ & + \left(\frac{a_{15}(\alpha_1 - a_{11})}{2} - \frac{a_{12}a_{25}}{2}\right)v^2 + \left(\frac{a_{16}(\alpha_1 - a_{11})}{6} - \frac{a_{12}a_{26}}{6}\right)u^3 \\ & + \left(\frac{a_{17}(\alpha_1 - a_{11})}{2} - \frac{a_{12}a_{27}}{2}\right)u^2v + \left(\frac{a_{18}(\alpha_1 - a_{11})}{2} - \frac{a_{12}a_{28}}{2}\right)uv^2 \\ & + \left(\frac{a_{19}(\alpha_1 - a_{11})}{6} - \frac{a_{12}a_{29}}{6}\right)v^3 + O((|U| + |V|)^4). \end{aligned} \quad (32b)$$

In order for map (31) to undergo Hopf bifurcation, the following discriminatory quantity  $a$  must not be zero [31]:

$$a = -\operatorname{Re}\left(\frac{(1-2\bar{\lambda})\bar{\lambda}^2}{1-\bar{\lambda}}\xi_{11}\xi_{20}\right) - \frac{1}{2}|\xi_{11}|^2 - |\xi_{02}|^2 + \operatorname{Re}(\bar{\lambda}\xi_{21}) \neq 0, \quad (33)$$

where

$$\xi_{20} = \frac{1}{8}\left((F_{UU} - F_{VV} + 2G_{UV}) + i'(G_{UU} - G_{VV} - 2F_{UV})\right), \quad (34a)$$

$$\xi_{11} = \frac{1}{4}\left((F_{UU} + F_{VV}) + i'(G_{UU} + G_{VV})\right), \quad (34b)$$

$$\xi_{02} = \frac{1}{8}\left((F_{UU} - F_{VV} - 2G_{UV}) + i'(G_{UU} - G_{VV} + 2F_{UV})\right), \quad (34c)$$

$$\xi_{21} = \frac{1}{16}\left((F_{UUU} + F_{UVV} + G_{UUV} + G_{Vvv}) + i'(G_{UUU} + G_{UVV} - F_{UUV} - F_{Vvv})\right), \quad (34d)$$

in which  $F = \frac{F_1}{a_{12}\alpha_2}$ ,  $G = \frac{G_1}{a_{12}\alpha_2}$ ,  $F_{UU} = \frac{\partial^2 F}{\partial U^2}|_{U=V=0}$ ,  $F_{UUU} = \frac{\partial^3 F}{\partial U^3}|_{U=V=0}$ , and likewise for all other similar terms. For the reason of simplification, we do not show the detailed calculations of  $F_{UU}$ ,  $F_{UUU}$ , etc. here.

Take the above calculations together, the following can be described. If the conditions (18), (19), (26), (29), and (33) establish, Hopf bifurcation takes place at  $(N_2, P_2)$ . Moreover, if  $a < 0$  and  $d > 0$  satisfy, an attracting invariant closed curve bifurcates from  $(N_2, P_2)$  for  $\tau > \tau_0$  (notice this statement is for  $(N, P, \tau)$  space). In such case,  $(N_2, P_2)$  loses its stability and the Hopf instability occurs.

### 3.3. Conditions for Turing instability

Spatially heterogeneous perturbations are introduced to perturb the stable homogeneous state  $(N_2, P_2)$ . Under the spatially heterogeneous perturbations, both  $\nabla_d^2 N_{(i,j,m)}$  and  $\nabla_d^2 P_{(i,j,m)}$  will not always be zero. Before we address the spatially heterogeneous perturbations, the eigenvalues of discrete Laplacian operator  $\nabla_d^2$  are determined. Considering the following equation

$$\nabla_d^2 X^{ij} + \lambda X^{ij} = 0, \quad (35)$$

with the periodic boundary conditions

$$X^{i,0} = X^{i,n}, \quad X^{i,1} = X^{i,n+1}, \quad X^{0,j} = X^{n,j}, \quad X^{1,j} = X^{n+1,j} \quad (36)$$

Applying the method described in Bai and Zhang [32], the eigenvalues of the operator can be solved and described as

$$\lambda_{kl} = 4(\sin^2 \phi_k + \sin^2 \phi_l), \quad (37)$$

in which  $\phi_k = \frac{(k-1)\pi}{n}$ ,  $\phi_l = \frac{(l-1)\pi}{n}$ , and  $k, l \in \{1, 2, 3, \dots, n\}$ .

Now considering spatially heterogeneous perturbations around the homogeneous state  $(N_2, P_2)$ , i.e.,

$$N_{(i,j,m)} = N_2 + \tilde{N}_{(i,j,m)}, \quad (38a)$$

$$P_{(i,j,m)} = P_2 + \tilde{P}_{(i,j,m)}, \quad (38b)$$

in which  $\tilde{N}_{(i,j,m)}$  and  $\tilde{P}_{(i,j,m)}$  are the perturbations on the prey density and the predator density in  $(i, j)$  site at  $m$ th iteration. Substituting Eqs. (38) into Eqs. (5), and noticing that

$$\nabla_d^2 N_{(i,j,m)} = \nabla_d^2 \tilde{N}_{(i,j,m)}, \quad (39a)$$

$$\nabla_d^2 P_{(i,j,m)} = \nabla_d^2 \tilde{P}_{(i,j,m)}, \quad (39b)$$

the following equations can be obtained,

$$\tilde{N}_{(i,j,m+1)} = a_{11} \left( \tilde{N}_{(i,j,m)} + \frac{\tau}{h^2} d_1 \nabla_d^2 \tilde{N}_{(i,j,m)} \right) + a_{12} \left( \tilde{P}_{(i,j,m)} + \frac{\tau}{h^2} d_2 \nabla_d^2 \tilde{P}_{(i,j,m)} \right) + O\left(\left(|\tilde{N}_{(i,j,m)}| + |\tilde{P}_{(i,j,m)}|\right)^2\right), \quad (40a)$$

$$\tilde{P}_{(i,j,m+1)} = a_{21} \left( \tilde{N}_{(i,j,m)} + \frac{\tau}{h^2} d_1 \nabla_d^2 \tilde{N}_{(i,j,m)} \right) + a_{22} \left( \tilde{P}_{(i,j,m)} + \frac{\tau}{h^2} d_2 \nabla_d^2 \tilde{P}_{(i,j,m)} \right) + O\left(\left(|\tilde{N}_{(i,j,m)}| + |\tilde{P}_{(i,j,m)}|\right)^2\right). \quad (40b)$$

When the perturbations are small,  $O((|\tilde{N}_{(i,j,m)}| + |\tilde{P}_{(i,j,m)}|)^2)$  can be ignored. Using the corresponding eigenfunction  $X_{kl}^{ij}$  of the eigenvalue  $\lambda_{kl}$  to multiply Eqs. (40) gets

$$X_{kl}^{ij} \tilde{N}_{(i,j,m+1)} = a_{11} X_{kl}^{ij} \tilde{N}_{(i,j,m)} + a_{12} X_{kl}^{ij} \tilde{P}_{(i,j,m)} + \frac{\tau}{h^2} a_{11} d_1 X_{kl}^{ij} \nabla_d^2 \tilde{N}_{(i,j,m)} + \frac{\tau}{h^2} a_{12} d_2 X_{kl}^{ij} \nabla_d^2 \tilde{P}_{(i,j,m)}, \quad (41a)$$

$$X_{kl}^{ij} \tilde{P}_{(i,j,m+1)} = a_{21} X_{kl}^{ij} \tilde{N}_{(i,j,m)} + a_{22} X_{kl}^{ij} \tilde{P}_{(i,j,m)} + \frac{\tau}{h^2} a_{21} d_1 X_{kl}^{ij} \nabla_d^2 \tilde{N}_{(i,j,m)} + \frac{\tau}{h^2} a_{22} d_2 X_{kl}^{ij} \nabla_d^2 \tilde{P}_{(i,j,m)}. \quad (41b)$$

Summing Eqs. (41) for all of  $i$  and  $j$  obtains

$$\sum_{i,j=1}^n X_{kl}^{ij} \tilde{N}_{(i,j,m+1)} = a_{11} \sum_{i,j=1}^n X_{kl}^{ij} \tilde{N}_{(i,j,m)} + a_{12} \sum_{i,j=1}^n X_{kl}^{ij} \tilde{P}_{(i,j,m)} + \frac{\tau}{h^2} a_{11} d_1 \sum_{i,j=1}^n X_{kl}^{ij} \nabla_d^2 \tilde{N}_{(i,j,m)} + \frac{\tau}{h^2} a_{12} d_2 \sum_{i,j=1}^n X_{kl}^{ij} \nabla_d^2 \tilde{P}_{(i,j,m)}, \quad (42a)$$

$$\sum_{i,j=1}^n X_{kl}^{ij} \tilde{P}_{(i,j,m+1)} = a_{21} \sum_{i,j=1}^n X_{kl}^{ij} \tilde{N}_{(i,j,m)} + a_{22} \sum_{i,j=1}^n X_{kl}^{ij} \tilde{P}_{(i,j,m)} + \frac{\tau}{h^2} a_{21} d_1 \sum_{i,j=1}^n X_{kl}^{ij} \nabla_d^2 \tilde{N}_{(i,j,m)} + \frac{\tau}{h^2} a_{22} d_2 \sum_{i,j=1}^n X_{kl}^{ij} \nabla_d^2 \tilde{P}_{(i,j,m)}. \quad (42b)$$

Let  $\tilde{N}_m = \sum_{i,j=1}^n X_{kl}^{ij} \tilde{N}_{(i,j,m)}$  and  $\tilde{P}_m = \sum_{i,j=1}^n X_{kl}^{ij} \tilde{P}_{(i,j,m)}$ , Eqs. (42) can be transformed into the following form under the consideration of periodic boundary conditions [33],

$$\tilde{N}_{m+1} = a_{11} \left( 1 - \frac{\tau}{h^2} d_1 \lambda_{kl} \right) \tilde{N}_m + a_{12} \left( 1 - \frac{\tau}{h^2} d_2 \lambda_{kl} \right) \tilde{P}_m, \quad (43a)$$

$$\tilde{P}_{m+1} = a_{21} \left( 1 - \frac{\tau}{h^2} d_1 \lambda_{kl} \right) \tilde{N}_m + a_{22} \left( 1 - \frac{\tau}{h^2} d_2 \lambda_{kl} \right) \tilde{P}_m. \quad (43b)$$

Eqs. (43) describe the dynamics of spatially heterogeneous perturbations integrating all the sites. If Eqs. (43) converge, the discrete predator-prey system will go back to the spatially homogeneous stationary state. Contrarily, the divergence of Eqs. (43) will lead to the breaking of the homogeneous state and the formation of Turing patterns. Applying the Jacobian matrix of Eq. (43),

$$J = \begin{pmatrix} a_{11} \left( 1 - \frac{\tau}{h^2} d_1 \lambda_{kl} \right) & a_{12} \left( 1 - \frac{\tau}{h^2} d_2 \lambda_{kl} \right) \\ a_{21} \left( 1 - \frac{\tau}{h^2} d_1 \lambda_{kl} \right) & a_{22} \left( 1 - \frac{\tau}{h^2} d_2 \lambda_{kl} \right) \end{pmatrix}. \quad (44)$$

Calculating the two eigenvalues of (44) as the following:

$$\lambda_{\pm}(k, l) = \frac{1}{2} \left( a_{11} + a_{22} - \frac{\tau}{h^2} (a_{11} d_1 + a_{22} d_2) \lambda_{kl} \right) \pm \frac{1}{2} \sqrt{\left( a_{11} - a_{22} - \frac{\tau}{h^2} (a_{11} d_1 - a_{22} d_2) \lambda_{kl} \right)^2 + 4 a_{12} a_{21} \left( 1 - \frac{\tau}{h^2} d_1 \lambda_{kl} \right) \left( 1 - \frac{\tau}{h^2} d_2 \lambda_{kl} \right)}. \quad (45)$$

When either  $|\lambda_+(k, l)| > 1$  or  $|\lambda_-(k, l)| > 1$  establishes with at least one group of  $k$  and  $l$  satisfying  $\lambda_{kl} \neq 0$ , Eqs. (43) will diverge. The divergence of Eqs. (43) suggests the occurrence of Turing instability. We define

$$Z(k, l) = \max(|\lambda_+(k, l)|, |\lambda_-(k, l)|), \quad (46)$$

and when

$$Z_m = \max_{k=1}^n \max_{l=1}^n Z(k, l) > 1 \quad ((k, l) \neq (1, 1)), \quad (47)$$

the Turing instability takes place. Thus, condition (47) describes the Turing instability criterion.

In literature, Rodrigues et al. [45] and White and White [46] have also determined the Turing instability criterion of coupled map lattice. Comparing the criterion determination for Turing instability in this research and in those two works, the following should be emphasized.

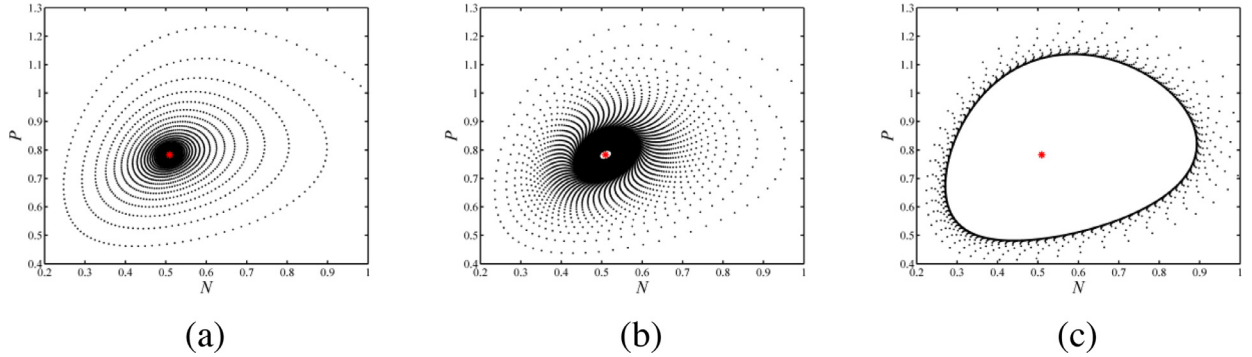


**Fig. 1.** Change of predator-prey dynamics with the variation of parameter  $\tau$ . The fixed point in  $N$ - $P$  space is (a) a stable focus at  $\tau = 0.3$ , (b) a weakly attracting focus at  $\tau = \tau_0 = 0.5075985$ , and (c) an unstable focus at  $\tau = 0.7$ .  $\tau_0$  is critical value for the occurrence of Hopf bifurcation.  $r = 0.5$ ,  $K = 2.2$ ,  $\beta = 0.6$ ,  $\varepsilon = 1$ ,  $B = 0.4$ ,  $w = 0.4$ ,  $\eta = 0.25$ ,  $d_1 = 0.01$ ,  $d_2 = 1$ , and  $h = 4$ .

- (1) These criteria are all obtained straightforwardly via applying relevant linear stability analysis to coupled map lattices.
- (2) The criterion determination in this research and in White and White is based on periodic boundary conditions. Differently, the criterion determination is independent on the boundary conditions in Rodrigues et al.
- (3) In handling the perturbations, this research integrates the perturbations in all sites; Rodrigues et al. expanded the perturbations into a Fourier-type generic solution; and White and White utilized the Fourier transformation.
- (4) The Turing instability criteria in Rodrigues et al. and White and White are given through either plus-one or minus-one bifurcation. Such two bifurcations can also occur in this research with the satisfaction of  $\lambda_+(k, l) > 1$  and  $\lambda_-(k, l) < -1$ . Condition (47) combines the two bifurcation cases into one inequality.
- (5) The Turing instability criteria in the three research works are all necessary and sufficient. Due to the uniqueness of sufficient and necessary condition, the three criteria should be equivalent if applied to the same coupled map lattice.

From the calculations in above three subsections, the conditions for pattern formation are found. The heterogeneous pattern formation occurs if one of the following conditions holds: (i) conditions (15) and (47) establish (pure Turing instability); (ii) When Hopf bifurcation occurs, conditions  $a < 0$ ,  $d > 0$ ,  $\tau > \tau_0$  and (47) establish (Hopf-Turing instability).

#### 4. Numerical simulations

Based on the theoretical conditions determined in Section 3, numerical simulations are performed in this section to demonstrate the bifurcations and the pattern formation of the discrete model. For the numerical simulations, parameter values are provided based on former research works [15,16]. In this research, we fix the values of the following parameters as  $\beta = 0.6$ ,  $\varepsilon = 1$ ,  $B = 0.4$ ,  $w = 0.4$ ,  $\eta = 0.25$ ,  $d_2 = 1$ , and shift the values of the other parameters  $r$ ,  $K$ ,  $d_1$ ,  $\tau$ , and  $h$ , to observe the dynamical variations in the discrete model. Moreover, to ensure non-negativity of  $N$  and  $P$  in the numerical simulations, the following two restrictions are made.

- (1) For Eqs. (3–4), the values of parameter  $\tau$ ,  $h$ ,  $d_1$ , and  $d_2$  must satisfy  $d_i\tau/h^2$  ( $i = 1, 2$ ) being less than 0.5 [47].
- (2) For Eqs. (5–6), let  $\xi_1 = \min_{\Omega}(f - gP/N)$ ,  $\xi_2 = \min_{\Omega}(\varepsilon g - \eta)$ , and  $\xi = \min(\xi_1, \xi_2)$ , where  $f$  and  $g$  are described by Eqs. (2),  $\Omega = \{(N, P) | 0 \leq N \leq K, 0 \leq P \leq K_P\}$  and  $K_P = \varepsilon \beta K/w\eta - (B + K)/w$ , then the value of parameter  $\tau$  should satisfy  $\tau < -1/\xi$ . It should be noticed that this restriction is very strong, therefore it can be slightly and properly relaxed if needed.

Fig. 1 shows the occurrence of Hopf bifurcation as the value of parameter  $\tau$  varies. According to the conditions in Section 3, the critical value for Hopf bifurcation can be determined as  $\tau_0 = 0.5075985$ . As shown in the  $N$ - $P$  space, when  $\tau \leq \tau_0$ , the stable stationary state is asymptotically stable (see Fig. 1a and b); otherwise, the stationary state becomes unstable and an attracting invariant closed curve emerges around it (see Fig. 1c). The attracting invariant curve leads to a dynamical state which is homogeneous in space and quasi-periodically oscillating in time.

Fig. 2 demonstrates  $Z(k, l)$  in four cases with the variations of parameter values. To better show the maximum value of function  $Z(k, l)$ , we particularly define  $Z_k = \max_{l=1}^n Z(k, l)$  and plot the curves of  $Z_k$ . In each case of Fig. 2, two aspects of dynamics are analyzed. First, we analyze whether the Hopf instability takes place. With the parametric conditions given for Fig. 2a and b, the moduli of the eigenvalues of  $(N_2, P_2)$  are 0.9988 and 0.9992, respectively. Therefore,  $(N_2, P_2)$  is stable and Hopf instability does not occur in both cases. Calculating the moduli of the eigenvalues for  $(N_2, P_2)$  in Fig. 2c and d, which are both larger than one, it is found that  $(N_2, P_2)$  is unstable. Further plotting the attractors in the  $N$ - $P$  space, we find attracting invariant curves (see Fig. 1c for example), which suggest the occurrence of Hopf instability in Fig. 2c and d. Second, the value of  $Z_m$  is calculated to determine whether the Turing instability occurs. In the four cases of Fig. 2, we have  $Z_m = 0.99877, 1.00081, 0.99991$  and  $1.00257$ , respectively. Fig. 2a and c show that Turing instability does not occur ( $Z_m < 1$ ), and the predator-prey dynamics in such cases will stabilize at the stationary state (Fig. 2a) or follow the quasi-periodic

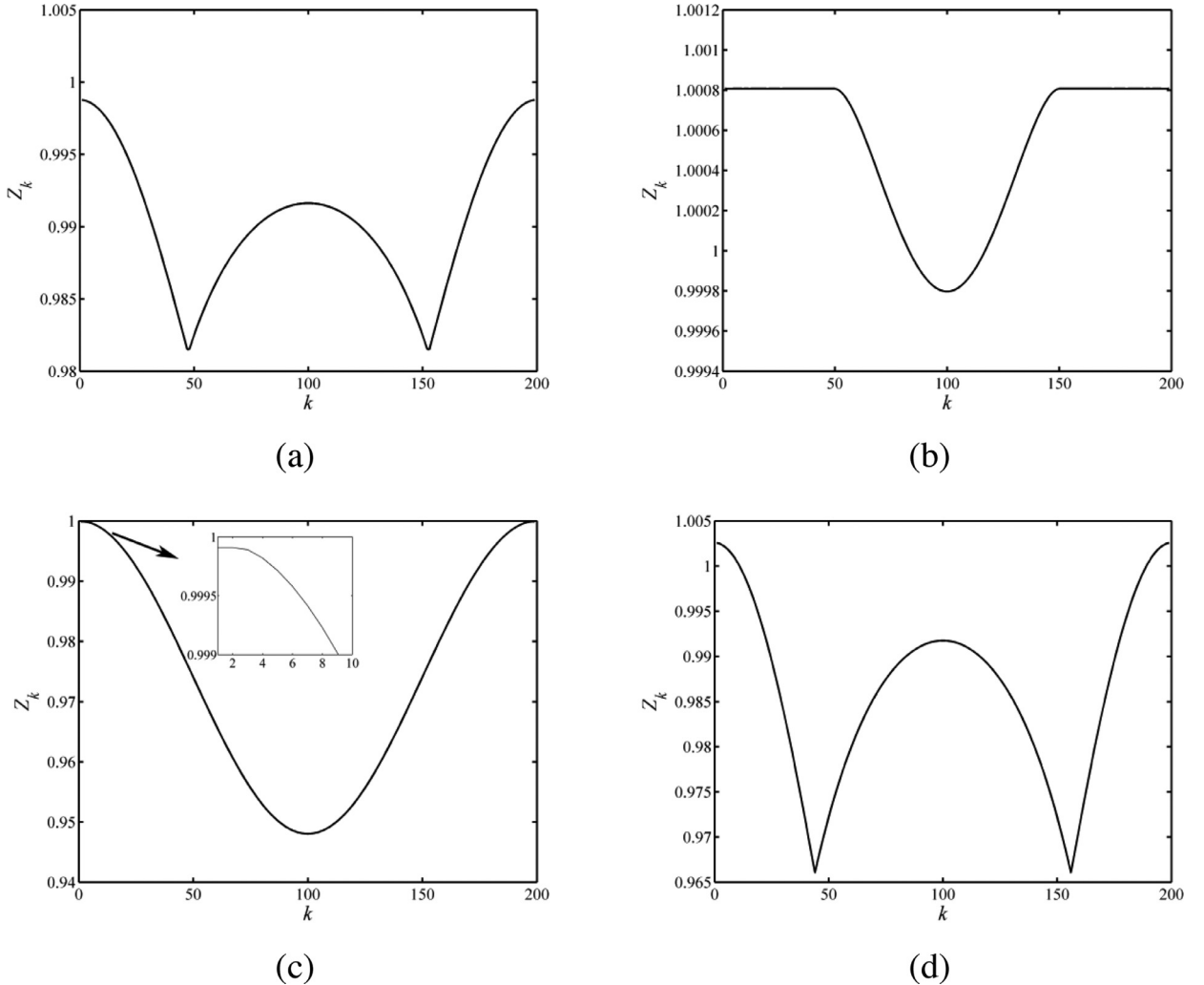


**Fig. 2.** Diagrams of  $Z_k$  in four cases. (a) and (b) are the cases of stable stationary state, whereas (c) and (d) are the cases of attracting invariant curve. (a)  $\tau = 0.3$ ,  $Z_m = 0.99877$ , (b)  $\tau = 0.1$ ,  $h = 1$ ,  $Z_m = 1.00081$ , (c)  $K = 2.6$ ,  $d_1 = 0.13$ ,  $\tau = 0.001$ ,  $h = 0.1$ ,  $Z_m = 0.99991$ , and (d)  $\tau = 0.7$ ,  $Z_m = 1.00257$ . The other parameter values in each graph are the same with that in Fig. 1.

oscillation (Fig. 2c). Fig. 2b and d show that the Turing instability takes place ( $Z_m > 1$ ). Combined with the analysis of Hopf instability, we know that two cases of Turing instability, pure Turing instability (Fig. 2b) and Hopf–Turing instability (Fig. 2d), are described. These two cases both suggest the pattern formation.

It is reasonable to numerically analyze the parameter space for pattern formation, as shown in Fig. 3. Fig. 3a displays a  $K$ - $d_1$  parameter space including four regions separated by the curves of Hopf bifurcation and Turing bifurcation. The curve of Hopf bifurcation is given by (19). Under the parametric conditions given for Fig. 3a, the curve of Hopf bifurcation can be obtained as  $K = 2.63$ . Based on the analysis in Section 3.3, the curve of Turing bifurcation is given by  $Z_m = \max_{k=1}^n \max_{l=1}^n Z(k, l) = 1$ . Since function  $Z_m$  is complicate, the specific expression for the curve of Turing bifurcation is hard to obtain and therefore is not presented here. The four regions divided in Fig. 3a describe four cases of predator–prey dynamics. Region I is the case of stable stationary state without Turing instability and Hopf instability; region II is the case of pure Turing instability; region III is the case of pure Hopf instability; region IV is the case of Hopf–Turing instability. When parameter values are located in region II or IV, the discrete model can generate spatially heterogeneous patterns. It should be noticed that the pure Hopf instability region may vanish as the parameter values shift, as shown in Fig. 3b. Under the parametric conditions given for Fig. 3b, there is no intersection between the curve of Hopf bifurcation and the curve of Turing bifurcation. In such case, Hopf instability always leads to Turing instability.

Great deals of numerical simulations are performed for the spatial pattern formation of the discrete model, based on the parameter values determined in regions II and IV. For pattern simulations, initial conditions are given by small randomly perturbing the homogeneous stationary state ( $N_2, P_2$ ). Many types of spatial patterns are found in the simulations, as classified in Figs. 4–10. Since the patterns of predator and prey always show the same distributions, we restrict our numerical

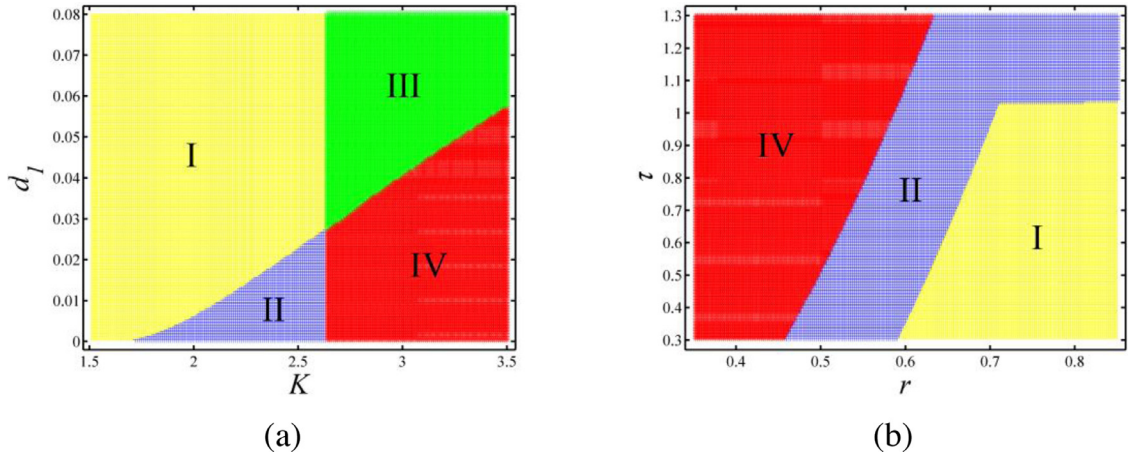


**Fig. 3.** Region diagrams shown in  $K$ - $d_1$  and  $r$ - $\tau$  parameter spaces. The regions are separated by the curves of Hopf bifurcation and Turing bifurcation. (a)  $r = 0.5$ ,  $\tau = 0.001$ ,  $h = 0.1$ , and (b)  $K = 2.2$ ,  $d_1 = 0.01$ ,  $h = 2$ . The other parameter values in each graph are the same with that in Fig. 1.

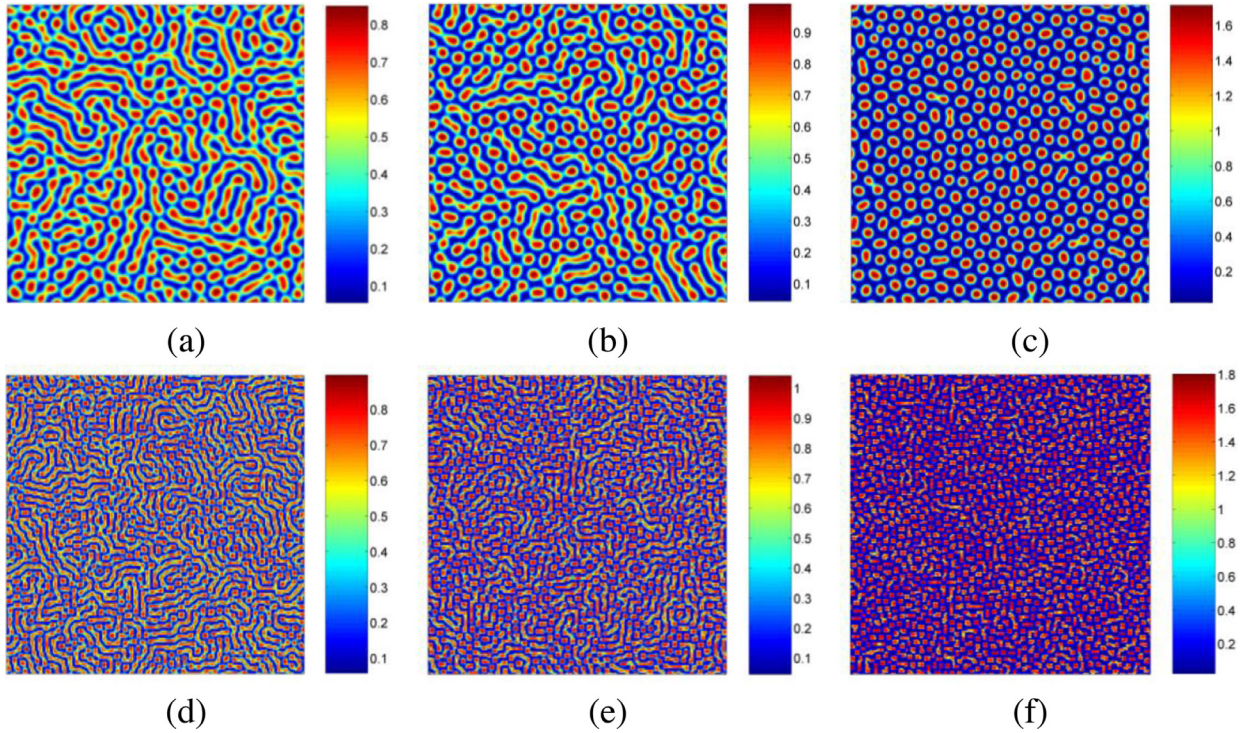
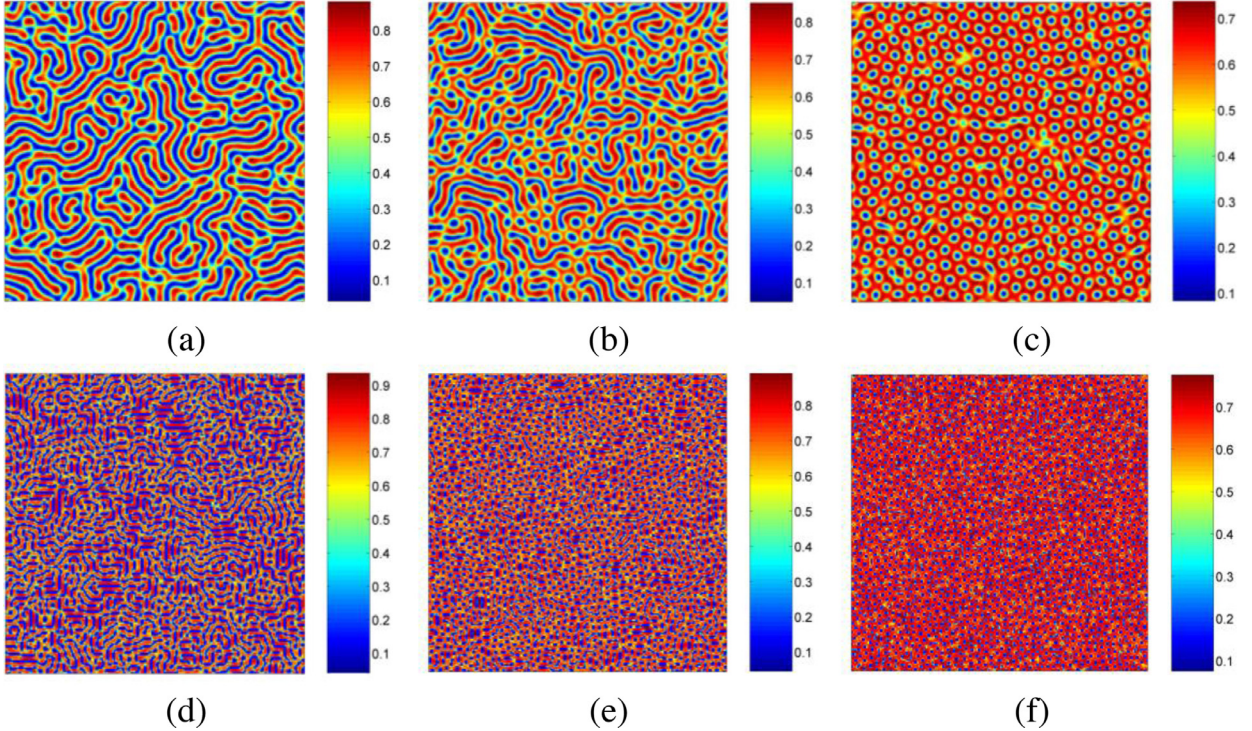


**Fig. 4.** Spatial patterns of prey with different values of  $K$ ,  $\tau$ , and  $h$ . The parameter values are shown in Table 1.  $n = 200$  and  $m = 20,000$  for all patterns.

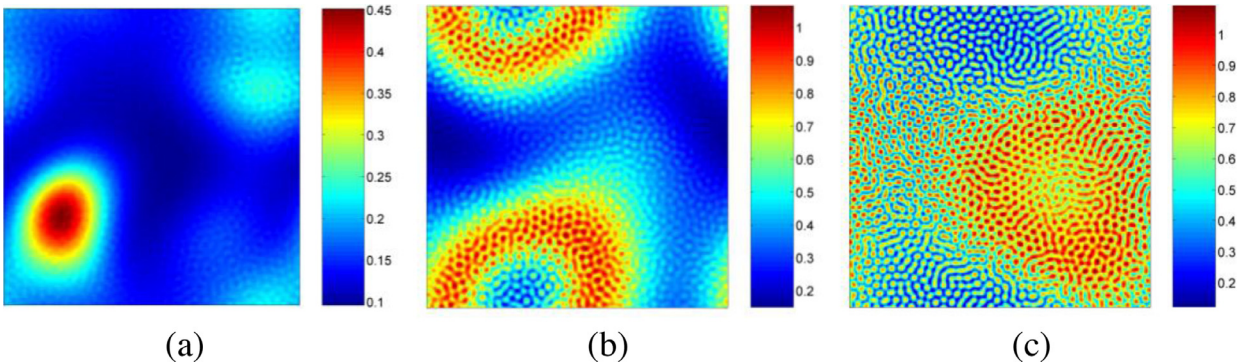
analysis to either predator patterns or prey patterns. As demonstrated in the following figures, the prey patterns are merely focused upon.

Fig. 4 shows the variations of prey patterns with parameter  $K$ , for two groups of  $\tau$  and  $h$ . As demonstrated in Fig. 4, increase of  $K$  value gradually breaks the stripes in the pattern into spots. This leads to a transition process from stripe-spot patterns to spot patterns. Simultaneously, as shown in Fig. 4, change of  $\tau$  and  $h$  influences the sizes of the stripes and spots in the patterns.

Fig. 5 shows the variations of prey patterns with parameter  $r$ , for  $\tau = 0.05$ ,  $h = 0.5$  and  $\tau = 0.1$ ,  $h = 1$ . A transition process from labyrinth pattern, to labyrinth-gap pattern, and to gap pattern can be found as the value of  $r$  rises. Meanwhile, enlarging values of  $\tau$  and  $h$  will reduce the stripe sizes in the labyrinth patterns or gap sizes in the gap patterns. Fig. 6 demonstrates the spatial patterns when  $r = 0.10, 0.12, 0.14$ , and the other parameter values are the same with that of Fig. 5d–f. These patterns are intermediate states between homogeneous state and stripe-spot patterns and only exist in a narrow



**Fig. 5.** Spatial patterns of prey with different values of  $r$ ,  $\tau$ , and  $h$ . The parameter values are shown in Table 2.  $n = 200$  and  $m = 20,000$  for all patterns.



**Fig. 6.** Spatial patterns of prey with different values of  $r$ . The parameter values are shown in Table 2.  $n = 200$  and  $m = 20,000$  for all patterns.

**Table 1**  
The parameter values applied for Fig. 4.

Parameters	$r$	$K$	$d_1$	$\tau$	$h$	The other parameters
Fig. 4a	0.2	2.2	0.01	0.05	0.5	$\beta = 0.6$ ;
Fig. 4b	0.2	2.4	0.01	0.05	0.5	$\varepsilon = 1$ ;
Fig. 4c	0.2	3.5	0.01	0.05	0.5	$B = 0.4$ ;
Fig. 4d	0.2	2.2	0.01	0.1	1	$w = 0.4$ ;
Fig. 4e	0.2	2.4	0.01	0.1	1	$\eta = 0.25$ ;
Fig. 4f	0.2	3.5	0.01	0.1	1	$d_2 = 1$

range of parameter  $r$  (with the other parameter values given in Table 2). With the increase of  $r$  value, these patterns will gradually change to stripe-spot patterns, which will then change to labyrinth patterns as described in Fig. 5d.

In the numerical simulations, we find that change of parameter  $d_1$  may fragment the prey patterns and increase the pattern irregularities. Figs. 7 and 8 show the formation of irregular stripe-spot patterns and irregular labyrinth patterns.

**Table 2**

The parameter values applied for Figs. 5 and 6.

Parameters	$r$	$K$	$d_1$	$\tau$	$h$	The other parameters
Fig. 5a	0.30	2.2	0.01	0.05	0.5	$\beta = 0.6$ ;
Fig. 5b	0.40	2.2	0.01	0.05	0.5	$\varepsilon = 1$ ;
Fig. 5c	0.50	2.2	0.01	0.05	0.5	$B = 0.4$ ;
Fig. 5d	0.30	2.2	0.01	0.1	1	$w = 0.4$ ;
Fig. 5e	0.40	2.2	0.01	0.1	1	$\eta = 0.25$ ;
Fig. 5f	0.50	2.2	0.01	0.1	1	$d_2 = 1$
Fig. 6a	0.10	2.2	0.01	0.1	1	
Fig. 6b	0.12	2.2	0.01	0.1	1	
Fig. 6c	0.14	2.2	0.01	0.1	1	

**Table 3**

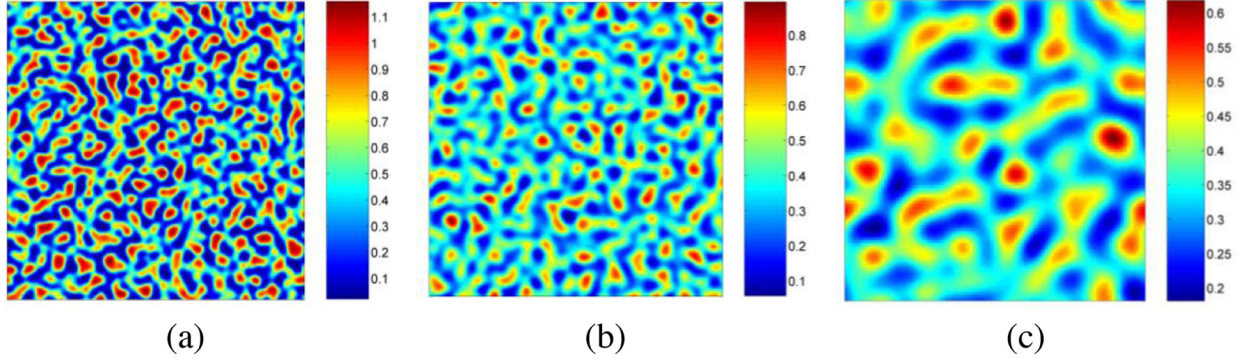
The parameter values applied for Figs. 7 and 8.

Parameters	$r$	$K$	$d_1$	$\tau$	$h$	The other parameters
Fig. 7a	0.2	2.2	0.001	0.01	0.2	$\beta = 0.6$ ;
Fig. 7b	0.2	2.2	0.002	0.01	0.2	$\varepsilon = 1$ ;
Fig. 7c	0.2	2.2	0.003	0.01	0.2	$B = 0.4$ ;
Fig. 8a	0.2	2.2	0.001	0.1	1	$w = 0.4$ ;
Fig. 8b	0.2	2.2	0.003	0.1	1	$\eta = 0.25$ ;
Fig. 8c	0.2	2.2	0.005	0.1	1	$d_2 = 1$

**Table 4**

The parameter values applied for Fig. 10.

Parameters	$r$	$K$	$d_1$	$\tau$	$h$	The other parameters
Fig. 10a	0.20	2.2	0.01	0.1	4	$\beta = 0.6$ ;
Fig. 10b	0.20	1.8	0.01	1	4	$\varepsilon = 1$ ;
Fig. 10c	0.20	2.5	0.01	1	4	$B = 0.4$ ;
Fig. 10d	0.20	4.8	0.01	1	4	$w = 0.4$ ;
Fig. 10e	0.20	2.2	0.01	1.43	4	$\eta = 0.25$ ;
Fig. 10f	0.20	2.2	0.01	1.5	4	$d_2 = 1$

**Fig. 7.** Irregular stripe-spot patterns with different values of  $d_1$ . The parameter values are shown in Table 3.  $n = 200$  and  $m = 20,000$  for all patterns.

Increasing  $d_1$  value can bring a transition from the stripe-spot patterns to spatially homogeneous state in Fig. 7. It can also reduce the pattern irregularities in Fig. 8 and result in a transition to regular labyrinth patterns.

When the parameters  $\tau$  and  $h$  take larger values than in above figures, new types of prey patterns can be found, as shown in Figs. 9 and 10. Fig. 9 shows two mosaic patterns, regular and irregular, when  $\tau = 1$  and  $h = 3.0, 3.5$ . The mosaic patterns compose of two or more interweaving patches. Fig. 10 shows spiral patterns of prey, in which spiral waves rotate around the focuses. This is a type of important patterns often recorded in the studies of predator-prey systems [4]. In this research, the spiral patterns present irregular properties and diverse appearances. Moreover, the spiral patterns may develop into circle pattern with parameter variations, as the spiral wave catches itself in the rotation (see Fig. 10f). In Fig. 10, six spiral and circle patterns are presented according to the degree of rotation, from barely rotating to the occurrence of circles. In numerical simulations, many more spiral and circle patterns are found, demonstrating complexity and diversity of the pattern formation of the predator-prey systems.

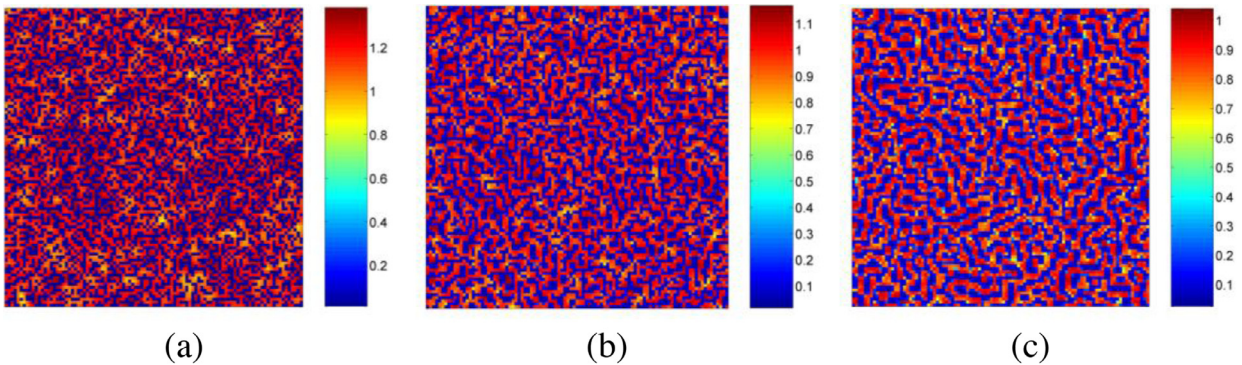


**Fig. 8.** Irregular labyrinth patterns with different values of  $d_1$ . The parameter values are shown in Table 3.  $n = 100$  and  $m = 20,000$  for all patterns.

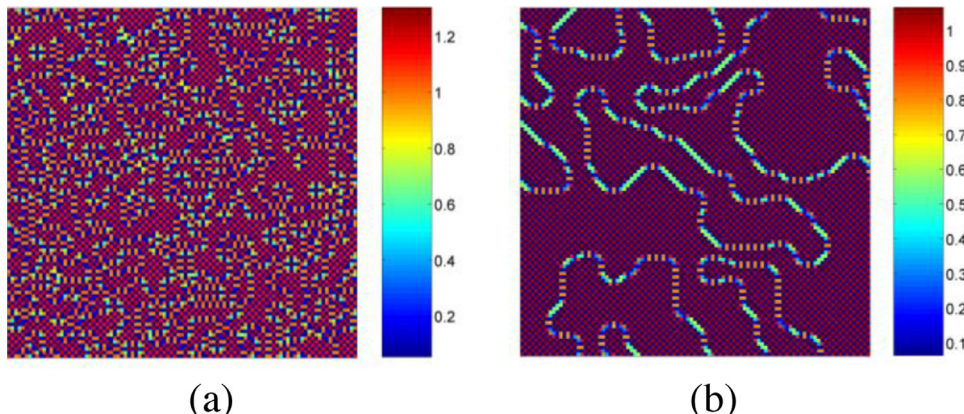


**Fig. 9.** Spatial patterns of prey with different values of  $h$ . (a)  $h = 3.0$ , (b)  $h = 3.5$ ,  $\tau = 1$ , and the other parameter values are the same with that of Fig. 4a.  $n = 100$  and  $m = 20,000$  for all patterns.

In the simulations, spatiotemporal chaos is found, playing a key role in the pattern formation. Fig. 11 is plotted to show the spatiotemporal chaos in the pattern formation. Generally, the chaos is characterized by the sensitivity to initial conditions. Therefore in plotting Fig. 11, two initial conditions with tiny difference between them are applied. It is shown that the dynamical behaviors at the same sites coincide at the beginning and diverge dramatically as time progresses, indicating the formation of two totally different patterns. This result suggests that the spatiotemporal chaos occurs and is responsible for the formation of complex irregular patterns.

## 5. Discussion

The discrete model developed in this research shows power in exhibiting diverse spatial patterns for the predator-prey system. Based on the numerical simulations, we find the patterns of spots, stripes, labyrinth, gaps, mosaics, spirals, and circles. Many intermediate patterns, such as stripe-spot patterns, labyrinth-spot patterns, labyrinth-gap patterns, etc., are also found in the pattern transitions resulting from parameter variations. These spatial patterns, regular and irregular, cover a majority of predator-prey pattern types recorded in literature [16,18,19,27].

The discrete model describes a space- and time-discrete Beddington–DeAngelis type predator-prey system, in which predator and prey may dwell in a fragmented habitat [27]. Accordingly, the pattern formation may reveal spatiotemporal predator-prey dynamics in patchy environment. Supposing each grid element in the discrete model mimics the properties of patchy environment and represents a patch which the predator and prey dwell in. Five aspects of ecological mechanisms can be discussed for the pattern formation of the discrete predator-prey system.

- (1) Inter-patch dispersal of predator and prey is the main reason making local population oscillations and resulting in the formation of complex patterns [27]. Such inter-patch interactions and consequent pattern formation play a key role in enhancing population persistence and affecting community functioning [48].
  - (2) Predator-prey interactions are an important factor driving heterogeneous distribution of predator and prey. Without predator-prey interactions, the system will inevitably converge to a homogeneous stationary state due to the inter-patch dispersal. Under the effect of predator-prey interactions, the predator and prey densities in patches can easily keep varying and stabilize in spatial heterogeneity.

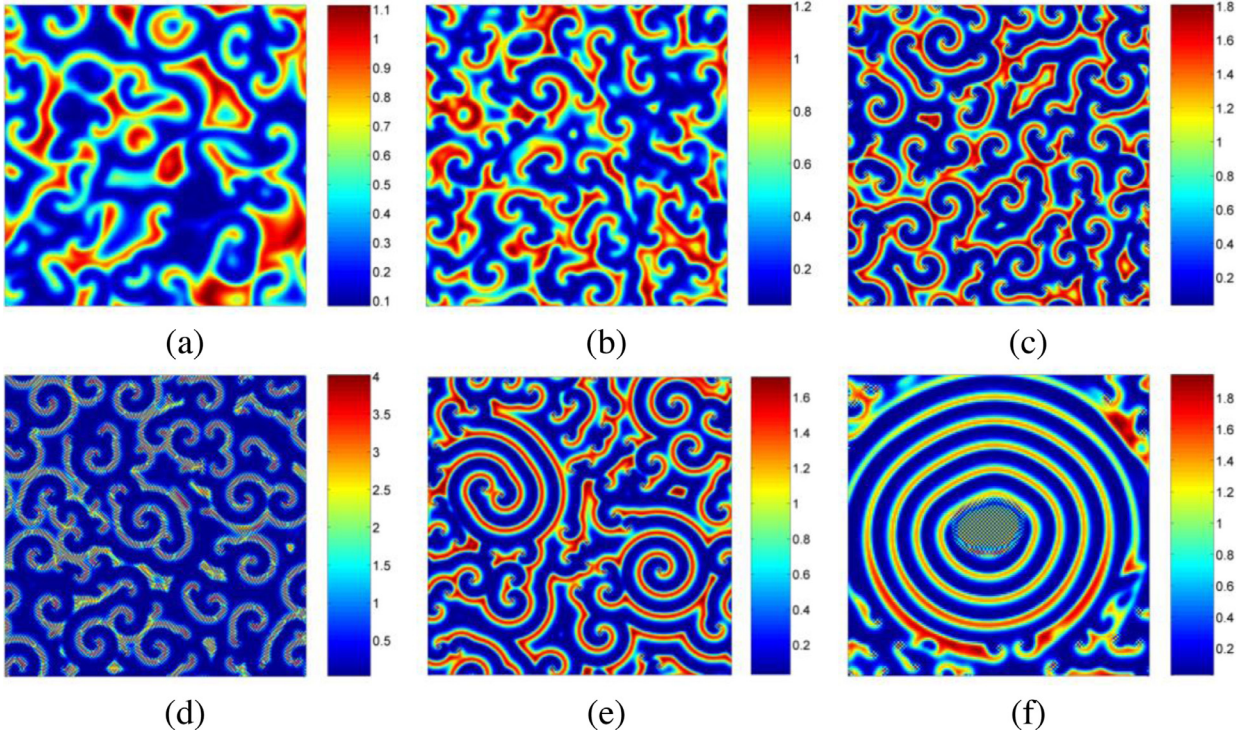


**Fig. 10.** Spiral and circle patterns of prey. The parameter values are shown in Table 4.  $n = 200$ , and  $m = 20,000$  for (a)~(e),  $m = 200,000$  for (f).

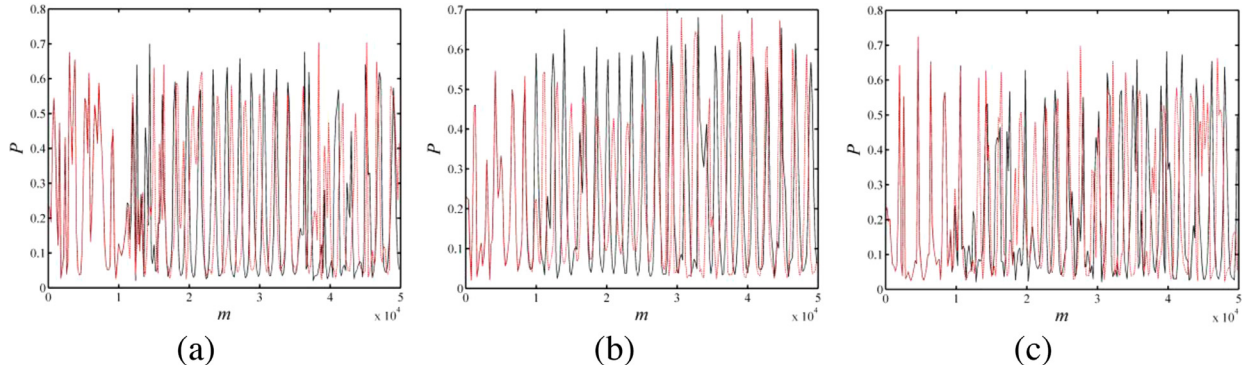


**Fig. 11.** Spatiotemporal chaos in the pattern formation. Two close initial conditions are applied (the difference of the two initial conditions is merely at one site, given by  $|N_1(50,50,0) - N_2(50,50,0)| = 0.0001$ ), resulting in totally different dynamical behaviors of prey. The  $P$ - $t$  diagrams are plotted for three sites, space coordinates of which are (a) (50, 150), (b) (150, 50), (c) (150, 150). The parameter values are the same with that in Fig. 10b.

- (3) The Beddington–DeAngelis functional response describes a feature of mutual interference between predators, which reduces the predation efficiency and increases the opportunity for predator-prey coexistence [49]. With the Beddington–DeAngelis functional response, the discrete system has two coexistent states, one of which is stationary and the other is oscillating. Turing instability on the two coexistent states leads to the formation of rich patterns.
- (4) Intra-specific competition hampers excessive aggregation of predator and prey in one patch. Thus, the intra-specific competition actually promotes the inter-patch dispersal of predator and prey. In literature, the intra-specific competition was considered as one of the most convincing mechanisms for spontaneous generation of patterns in a homogeneous environment [2].
- (5) The grid element in the discrete model has perfect square geometry, but the emerging spatial patterns hold almost no sign of the grid element structure. This result was also observed by Rodrigues et al. [27]. They suggested that “the effect of the self-organized system’s dynamics resulting in pattern formation is usually stronger than the effect of the underlying environmental structure” [27].

Under the combined effects of the ecological mechanisms, diverse complex predator-prey patterns are self-organized, as described in Section 4. The various spatial patterns describe many coexistent states of predator and prey in space, maintaining the stability of the predator-prey system. Notice that the self-organization of each pattern is after a long evolution of dynamics. Therefore, the variety of patterns also reflects many possible evolutionary processes of the predator-prey system.

When parameter variations occur in response to internal changes or external disturbances, transition of patterns can be found in the discrete predator-prey system. As demonstrated in Section 4, various pattern transitions can take place corresponding to the variations of different parameters. Based on the simulation results in this research, the following pattern transitions can be addressed.

- (1) Increases of  $r$  value leads to faster prey growth, promoting the dispersal of prey to neighboring patches. Correspondingly, the prey population can occupy more patches in space. This causes the transition from stripe-spot patterns to gap patterns, as shown in Figs. 5 and 6.
- (2) Rise of  $K$  value enables more prey individuals aggregating in one patch, enhancing the prey density and weakening the prey diffusion. This reduces the patches which prey occupy and consequently, leads to a transition from stripe-spot patterns to spot patterns, as shown in Fig. 4.
- (3) Variation of  $d_1$  value changes the diffusion capability of prey and influences the diffusion process. When  $d_1$  value gets smaller, the difference of dynamics between patches increases gradually. Eventually, it will cause the emergence of irregularity in the patterns due to weak diffusion, as shown in Figs. 7 and 8.
- (4) Enlarging the values of  $\tau$  and  $h$  can reduce the pattern size, but not change the pattern type, as shown in Figs. 4–8. Moreover, when the pattern size becomes minimal, mosaic patterns take place, as shown in Fig. 9.

The pattern transitions described above occur under pure Turing instability and have a characteristic of gradual change. When parameter variations cause the system dynamics changing from region II to region IV (see Fig. 3), a sudden shift of patterns may emerge and make the patterns transitioning to spirals or circles. As an important phenomenon, pattern transitions have been widely recorded in literature, reflecting how the predator-prey system responds to environmental fluctuations [27,36].

Two nonlinear mechanisms, pure Turing instability and Hopf-Turing instability, are found for the pattern formation of the discrete predator-prey system. The theory of Turing instability was initially proposed by Alan Turing [34] and has been widely employed to investigate the Turing pattern formation in reality [35,36]. In this research, pure Turing instability induces spatial symmetry breaking at the stable homogeneous stationary state, whereas Hopf-Turing instability induces spatial symmetry breaking at the homogeneous oscillating states. The patterns self-organized under the two instability mechanisms can be classified into two kinds, stationary patterns and oscillatory patterns. Oscillatory patterns include the spiral and circle patterns, and stationary patterns include the other patterns. In the stationary patterns, the spatial distribution of predator and prey keeps stationary and the system dynamics will not change with time. In the oscillatory patterns, the dynamics of predator and prey is always varying spatially and temporally. One of important characteristics of the oscillatory patterns is spatiotemporal chaos, which results in the formation of complex and diverse spiral/circle patterns. The spatiotemporal chaos has been widely described in literature, playing a vital role in the spatiotemporal organization of ecological systems [8,27,50]. Moreover, some researchers suggested that ecological systems with chaotic dynamics have a greater potential for adapting to changing environmental conditions than nonchaotic ones [50].

The discrete model in this research is developed via discretizing a continuous reaction-diffusion predator-prey model, which has been investigated by Wang et al. [15]. Compared with Wang's work, this research shows three advantages in describing pattern formation. First, the discrete model shows similar dynamical characteristics with Wang's model. By comparison, the similarity reflects in stationary states, bifurcations, and pattern formations [15]. When the parameter  $\tau$  becomes smaller, the dynamics of the two models gets closer. Second, the discrete model exhibits new dynamics never predicted by Wang's model. As widely known, an essential characteristic of discrete models is to produce very complex dynamical behaviors [22–24]. The discrete model shows complexity of dynamics, as demonstrated by the formation of diverse patterns. Third, the discrete model takes a nonlinear relationship between the dispersal stage and the reaction stage, as shown in Eqs. (3–6). Many research works have demonstrated that such nonlinear relationship is important for the spatiotemporal pattern formation of coupled map lattices [8,9,27,45]. Actually, in the development of coupled map lattices, a linear additive relationship is often taken as well [33,51]. Applying Euler discretization on Eqs. (1), the linear additive relationship between the two stages can be explicitly described by the following equations,

$$N_{(i,j,m+1)} = f_1(N_{(i,j,m)}, P_{(i,j,m)}) + \frac{\tau}{h^2} d_1 \nabla_d^2 N_{(i,j,m)}, \quad (48a)$$

$$P_{(i,j,m+1)} = g_1(N_{(i,j,m)}, P_{(i,j,m)}) + \frac{\tau}{h^2} d_2 \nabla_d^2 P_{(i,j,m)}. \quad (48b)$$

in which  $f_1$  and  $g_1$  are described by Eqs. (6). Eqs. (48) have a discrete analogue of the continuous reaction-diffusion model, and can be also used to investigate the spatiotemporal pattern formation of the predator-prey system. However, as suggested by Hassell et al. [52], the coupled map lattice model with such formulation fails to segregate the processes of reaction and dispersal. Consequently, the same individuals are allowed to die and disperse in the same generation. This may lead to counter-intuitive results, such as the production of negative local population densities at some extreme cases [51,52].

Previously, many research works have been done on the formation of complex patterns of predator-prey systems. For example, Wang and Wang investigated the transition from wave pattern to stationary pattern in a Holling-III type predator-prey system [53], Tang and Song studied the Hopf-Turing instability and spatial pattern formation in a delayed diffusive predator-prey system with herd behavior [54], Haque explored the self-organization of many complex patterns in a Beddington-DeAngelis predator-prey system [19], and so on. In comparing with former theoretical works, the improvement of this research may reflect in the following aspects. First, relying on the same ecological mechanisms with the continuous model proposed by Wang et al. [15], the discrete model reveals more complicate and richer spatial patterns. Extra ecological mechanisms, such as white noise [17], cross diffusion [16], need not be introduced in this research for explaining the emergence of these patterns. Second, the discrete model developed further bridges the continuous models and the discrete models. Likewise, similar approach can be made to other continuous models. Third, the discrete model is given by a coupled map lattice; for such coupled map lattice, an applicable method of quantitatively determining the pattern formation conditions is provided in this research.

In this research, the spatial predator-prey patterns are obtained under Beddington-DeAngelis functional response, which is one of the most important functional responses and has been widely studied [15,17,19,49]. Many research works demonstrated that the Beddington-DeAngelis functional response is very important for the predator-prey systems exhibiting dynamical complexity [15,17,19]. Especially in Haque's work [19], he found the Beddington-DeAngelis type predator-prey system can generate various instability mechanisms, including Hopf-Turing instability, pitchfork-Turing instability, Bogdanov-Takens-Turing instability, etc. It should be noticed that the development and analysis of the discrete model in this research do not rely on specific functional response of predation. Therefore, many other functional responses of predation can be also considered in the discrete model for investigating more pattern formations of the predator-prey systems.

## 6. Conclusions

A space- and time- discrete model is developed in this research for studying the pattern formation of predator-prey systems. The development of the model is based on discretization of a former continuous predator-prey model and application of a coupled map lattice framework. The discrete model takes a nonlinear relationship between the predator-prey “reaction” stage and the dispersal stage. With the employment of the discrete model, a majority of patterns are found for the predator-prey system with Beddington-DeAngelis functional response. With the findings of this research, the following concluding remarks can be made.

- (1) Pure Turing instability and Hopf-Turing instability are two nonlinear mechanisms for the pattern formation. With the conditions calculated for Turing instability and Hopf instability, the parameter regions for pattern formation are quantitatively determined. When the parameter data are given in region IV, the occurrence of Hopf-Turing instability leads to the formation of complex patterns with spatiotemporal chaos.
- (2) Relying on the nonlinear mechanisms of the discrete model, regular and irregular patterns of spots, stripes, labyrinth, gaps, mosaics, spirals, circles, and many intermediate patterns are found. These patterns are also recorded in literature and have realistic ecological significances for predator-prey systems. Like many studies in literature, pattern transitions with parameter variations are also found based on the discrete model.
- (3) The discrete model shows power in describing the pattern formation of predator-prey systems. Its mechanisms provide explanations for the complexity of patterns and pattern transitions. The investigation of this research contributes to a better understanding on the spatiotemporal complexity of predator-prey systems with Beddington-DeAngelis functional response.

## Acknowledgments

The authors would like to acknowledge with great gratitude for the supports of Chinese Natural Science Foundation (Project 39560023 to H.Z.), National Special Water Programs (No. 2009ZX07210-009, No. 2015ZX07203-011, No. 2015ZX07204-007), Department of Environmental Protection of Shandong Province (SDHBPJ-ZB-08), the China Scholarship Council (No. 201206730024), and to the University of Regina.

## References

- [1] Cobbold CA, Lutscher F, Sherratt JA. Diffusion-driven instabilities and emerging spatial patterns in patchy landscapes. *Ecol Complexity* 2015;24:69–81.
- [2] Guin LN. Spatial patterns through Turing instability in a reaction-diffusion predator-prey model. *Math Comput simul* 2015;109:174–85.
- [3] Kondo S, Miura T. Reaction-diffusion model as a framework for understanding biological pattern formation. *Science* 2010;329:1616–20.
- [4] Gurney WSC, Veitch AR, Cruickshank I, McGeachin G. Circles and spirals: Population persistence in a spatially explicit predator-prey model. *Ecology* 1998;79:2516–30.
- [5] Klausmeier CA. Regular and irregular patterns in semiarid vegetation. *Science* 1999;284:1826–8.
- [6] Borgogno F, D'Odorico P, Laio F, Ridolfi L. Mathematical models of vegetation pattern formation in ecohydrology. *Rev Geophys* 2009;47 RG1005.
- [7] Wang W, Liu Q-X, Jin Z. Spatiotemporal complexity of a ratio-dependent predator-prey system. *Phys Rev E* 2007;75:051913.
- [8] Mistro DC, Rodrigues LAD, Petrovskii S. Spatiotemporal complexity of biological invasion in a space- and time-discrete predator-prey system with the strong Allee effect. *Ecol Complexity* 2012;9:16–32.
- [9] Punithan D, Kim DK, McKay RIB. Spatio-temporal dynamics and quantification of daisyworld in two-dimensional coupled map lattices. *Ecol Complexity* 2012;12:43–57.
- [10] Taylor AD. Metapopulations, dispersal, and predator-prey dynamics: an overview. *Ecology* 1990;71:429–33.

- [11] Briggs CJ, Hoopes MF. Stabilizing effects in spatial parasitoid–host and predator–prey models: a review. *Theor Popul Biol* 2004;65:299–315.
- [12] Yang R. Hopf bifurcation analysis of a delayed diffusive predator–prey system with nonconstant death rate. *Chaos, Solitons Fract* 2015;81:224–32.
- [13] Hu D, Cao H. Bifurcation and chaos in a discrete-time predator–prey system of Holling and Leslie type. *Commun Nonlinear Sci Numer Simul* 2015;22:702–15.
- [14] Zhang H, Huang T, Dai L. Nonlinear dynamic analysis and characteristics diagnosis of seasonally perturbed predator–prey systems. *Commun Nonlinear Sci Numer Simul* 2015;22:407–19.
- [15] Wang W, Zhang L, Xue Y, Jin Z. Spatiotemporal pattern formation of Beddington–DeAngelis-type predator–prey model. arXiv preprint 2008; arXiv: 0801.0797v1. www.arxiv.org.
- [16] Wang W, Lin Y, Zhang L, Rao F, Tan Y. Complex patterns in a predator–prey model with self and cross-diffusion. *Commun Nonlinear Sci Numer Simul* 2011;16:2006–15.
- [17] Zhang XC, Sun GQ, Jin Z. Spatial dynamics in a predator–prey model with Beddington–DeAngelis functional response. *Phys Rev E* 2012;85:021924.
- [18] Xue L. Pattern formation in a predator–prey model with spatial effect. *Phys A* 2012;391:5987–96.
- [19] Haque M. Existence of complex patterns in the Beddington–DeAngelis predator–prey model. *Math Biosci* 2012;239:179–90.
- [20] Comer P, Faber-Langendoen D, Evans R, Gawler S, Josse C, Kittel G, et al. Ecological systems of the united states: a working classification of U.S. terrestrial systems. Arlington, Virginia: NatureServe; 2003.
- [21] Domokos G, Scheuring I. Discrete and continuous state population models in a noisy world. *J Theor Biol* 2004;227:535–45.
- [22] Liu X, Xiao D. Complex dynamic behaviors of a discrete-time predator–prey system. *Chaos, Solitons Fract* 2007;32:80–94.
- [23] Jing Z, Yang J. Bifurcation and chaos in discrete-time predator–prey system. *Chaos, Solitons Fract* 2006;27:259–77.
- [24] May RM. Simple mathematical models with very complicated dynamics. *Nature* 1976;261:459–67.
- [25] Saratchandran PP, Ajithprasad KC, Harikrishnan KP. Numerical exploration of the parameter plane in a discrete predator–prey model. *Ecol Complexity* 2015;21:112–19.
- [26] Ermentrout GB, Edelstein-Keshet L. Cellular automata approaches to biological modeling. *J Theor Biol* 1993;160:97–133.
- [27] Rodrigues LAD, Mistro DC, Petrovskii S. Pattern formation in a space- and time-discrete predator-prey system with a strong Allee effect. *Theor Ecol* 2012;5:341–62.
- [28] Alonso D, Bartumeus F, Catalan J. Mutual interference between predators can give rise to Turing spatial patterns. *Ecology* 2002;83:28–34.
- [29] Wang Q, Fan M, Wang K. Dynamics of a class of nonautonomous semi-ratio-dependent predator–prey systems with functional responses. *J Math Anal Appl* 2003;278:443–71.
- [30] Nayfeh AH, Balachandran B. Applied nonlinear dynamics: analytical, computational, and experimental methods. Wiley Interscience; 1995.
- [31] Guckenheimer J, Holmes P. Nonlinear oscillations, dynamical systems and bifurcations of vector fields. NY: Springer-Verlag; 1983.
- [32] Bai L, Zhang G. Nontrivial solutions for a nonlinear discrete elliptic equation with periodic boundary conditions. *Appl Math Comput* 2009;210:321–33.
- [33] Han Y-T, Han B, Zhang L, Xu L, Li M-F, Zhang G. Turing instability and wave patterns for a symmetric discrete competitive Lotka–Volterra system. *WSEAS Trans Math* 2011;10:181–9.
- [34] Turing AM. The chemical basis of morphogenesis. *philosophical transactions of the royal society of london. Series B* 1952;237:37–72.
- [35] Silva FDS, Viana RL, Prado TDL, Lopes SR. Characterization of spatial patterns produced by a Turing instability in coupled dynamical systems. *Commun Nonlinear Sci Numer Simul* 2014;19:1055–71.
- [36] Wang W, Lin Y, Yang F, Zhang L, Tan Y. Numerical study of pattern formation in an extended Gray–Scott model. *Commun Nonlinear Sci Numer Simul* 2011;16:2016–26.
- [37] Neubert MG, Kot M, Lewis MA. Dispersal and pattern formation in a discrete-time predator-prey model. *Theor Popul Biol.* 1995;48:7–43.
- [38] Kaneko K. Overview of coupled map lattices. *Chaos* 1992;2:279–82.
- [39] RV Solé, Bascompte J, Valls J. Nonequilibrium dynamics in lattice ecosystems: chaotic stability and dissipative structures. *Chaos* 1992;2:387–95.
- [40] Denaro G, Valenti D, Spagnolo B, Bonanno A, Basilone G, Mazzola S, et al. Dynamics of two picophytoplankton groups in Mediterranean Sea: analysis of the deep chlorophyll maximum by a stochastic advection-reaction-diffusion model. *PLoS one* 2013;8:e66765.
- [41] Denaro G, Valenti D, La Cognata A, Spagnolo B, Bonanno A, Basilone G, et al. Spatio-temporal behaviour of the deep chlorophyll maximum in Mediterranean Sea: Development of a stochastic model for picophytoplankton dynamics. *Ecol Complexity* 2013;13:21–34.
- [42] Valenti D, Denaro G, Spagnolo B, Conversano F, Brunet C. How diffusivity, thermocline and incident light intensity modulate the dynamics of deep chlorophyll maximum in Tyrrhenian sea. *PLoS one* 2015;10:e0115468.
- [43] Valenti D, Fiasconaro A, Spagnolo B. Role of the colored noise in spatio-temporal behavior of two competing species. *Fluctuation Noise Lett* 2005;5:L337–42.
- [44] Fiasconaro A, Valenti D, Spagnolo B. Nonmonotonic pattern formation in three species Lotka–Volterra system with colored noise. *Fluctuation Noise Lett* 2005;5:L305–11.
- [45] Rodrigues LAD, Mistro DC, Petrovskii S. Pattern formation, long-term transients, and the Turing–Hopf bifurcation in a space-and time-discrete predator-prey system. *Bull Math Biol* 2011;73:1812–40.
- [46] White SM, White KAJ. Relating coupled map lattices to integro-difference equations: dispersal-driven instabilities in coupled map lattices. *J Theor Biol* 2005;235:463–75.
- [47] Banerjee M. Comments on LN Guin, M. Haque, PK Mandal, The spatial patterns through diffusion-driven instability in a predator–prey model. *Appl. Math. Model.* 2012;36:1825–41 *Applied Mathematical Modelling* 2015; 1: 297–299.
- [48] Hassell MP, Comins HN, May RM. Spatial structure and chaos in insect population dynamics. *Nature* 1991;353:255–8.
- [49] Beddington JR. Mutual interference between parasites or predators and its effect on searching efficiency. *J Anim Ecol* 1975;44:331–40.
- [50] Medvinsky AB, Petrovskii SV, Tikhonova IA, Malchow H, Li B. Spatiotemporal complexity of plankton and fish dynamics. *SIAM Rev* 2002;44:311–70.
- [51] Bascompte J, RV Solé. Spatially induced bifurcations in single-species population dynamics. *J Anim Ecol* 1994;63:256–64.
- [52] Hassell MP, Miramontes O, Rohani P, May RM. Appropriate formulations for dispersal in spatially structured models: comments on Bascompte & Solé. *J Anim Ecol* 1995;64:662–4.
- [53] Wang C, Wang L. Transition from wave pattern to stationary pattern in a spatial predator-prey system with delay. *Chaos, Solitons Fract* 2015;78:156–61.
- [54] Tang X, Song Y. Stability, Hopf bifurcations and spatial patterns in a delayed diffusive predator–prey model with herd behavior. *Appl Math Comput* 2015;254:375–91.